

Symmetry-protected topological states for interacting fermions in alkaline-earth-like atoms

Xiaofan Zhou,^{1,2} Jian-Song Pan,^{3,4} Zheng-Xin Liu,^{5,6,*} Wei Zhang,^{5,6,†} Wei Yi,^{3,4,‡} Gang Chen,^{1,2,§} and Suotang Jia^{1,2}

¹State Key Laboratory of Quantum Optics and Quantum Optics Devices,
Institute of Laser spectroscopy, Shanxi University, Taiyuan 030006, P. R. China

²Collaborative Innovation Center of Extreme Optics,
Shanxi University, Taiyuan, Shanxi 030006, China

³Key Laboratory of Quantum Information, University of Science and Technology of China, CAS, Hefei, Anhui, 230026, China

⁴Synergetic Innovation Center of Quantum Information and Quantum Physics,
University of Science and Technology of China, Hefei, Anhui 230026, China

⁵Department of Physics, Renmin University of China, Beijing 100872, China

⁶Beijing Key Laboratory of Opto-electronic Functional Materials and Micro-nano Devices,
Renmin University of China, Beijing 100872, China

(Dated: January 17, 2017)

We discuss the quantum simulation of symmetry-protected topological (SPT) states for interacting fermions in quasi-one-dimensional gases of alkaline-earth-like atoms such as ^{173}Yb . Taking advantage of the separation of orbital and nuclear-spin degrees of freedom in these atoms, we consider Raman-assisted spin-orbit couplings in the clock states, which, together with the spin-exchange interactions in the clock-state manifolds, give rise to SPT states for interacting fermions. We numerically investigate the effects of bulk interactions on the topological properties of the system, characterize the interaction-induced topological phase boundaries, and map out the phase diagram. The interaction-induced topological phase transition can be probed by measuring local density distribution of the topological edge modes.

Introduction.— The study of symmetry-protected topological (SPT) phases has significantly improved our understanding of topological matters [1, 2]. In contrast to intrinsic topological orders with long-range entanglements [3–5], SPT phases feature short-range-entangled ground states with bulk gaps, and can have non-trivial edge excitations as long as the protecting symmetries are not broken. Notable examples of SPT phases range from the Haldane phase in one dimension for interacting spin systems [6], to topological insulators for free fermions in higher dimensions [7–11]. Apart from these well-known cases, theoretically, SPT phases should also exist for interacting fermions, although an experimental realization of such a state is still lacking.

In this work, we discuss the quantum simulation of SPT states for interacting fermions using alkaline-earth-like atoms. With two valence electrons, these atoms feature long-lived excited states and fermionic isotopes with non-zero nuclear spins. The nuclear- and the orbital-degrees of freedom are decoupled in the ground 1S_0 ($|g\rangle$) and the meta-stable excited 3P_0 ($|e\rangle$) manifolds, which enables flexible control of these so-called clock states. While the high level of quantum control has led to numerous applications in quantum metrology, quantum information and quantum simulation using the clock states [12–24], the recently discovered orbital Feshbach resonance in ^{173}Yb atoms further enriches the available toolbox, offering exciting possibilities of simulating strongly interacting fermionic systems using these atoms [25–27].

Taking advantage of these features and, in particular,

making use of the spin-exchange interactions in the clock states [18–20], we show that an SPT order for interacting fermions can be realized in a quasi-one-dimensional (1D) cold gas of alkaline-earth-like atoms. The SPT state derives from that of the chiral unitary AIII class with Z classification in the non-interacting limit, which reduces to Z_4 classes in the presence of symmetry-preserving interactions [28]. In quasi-1D, the interactions can be tuned via the magnetic field through the orbital Feshbach resonance, or via the transverse trapping potential through the confinement-induced resonance [29]. We reveal the existence of interaction-induced topological phase transitions by mapping out the phase diagram, and characterize the impact of interactions on the topological properties of the system. The topological phase transition, as well as the effects of interaction on the SPT state, can be probed by detecting the local occupation of the clock states at the edges. Our results open up the avenue of simulating SPT states for interacting fermions, and for studying SPT classifications using cold atoms.

Model.— We consider a quasi-1D cold atomic gas of alkaline-earth-like atoms trapped in an optical lattice potential along the axial direction, and tightly confined in the transverse directions. As illustrated in Fig. 1, a pair of blue-detuned Raman lasers simultaneously couple nuclear spin states $\{|g \downarrow\rangle, |g \uparrow\rangle\}$ in the $|g\rangle$, and $\{|e \downarrow\rangle, |e \uparrow\rangle\}$ in the $|e\rangle$ orbitals, respectively. The Rabi frequencies of the two lasers forming the Raman processes are, respectively, $\Omega_1(x) = \Omega_1 \cos(k_0 x)$ and $\Omega_2 \exp(ik_0 y)$, which, in addition to imposing Raman-assisted spin-orbit couplings (SOCs) on the nuclear spins, give rise to 1D optical

lattice potentials for the states $\{|\alpha \uparrow\rangle, |\alpha \downarrow\rangle\}$ ($\alpha = g, e$). When the Raman lasers are at a magic wavelength, the optical lattice potentials, as well as the effective Rabi frequencies of the Raman processes should be the same for the $|g\rangle$ and the $|e\rangle$ orbitals. Such a condition can be satisfied, for example, at the magic wavelength of $\sim 550\text{nm}$ for ^{173}Yb atoms [31]. Under such a setup, the single-particle Hamiltonian can be written as

$$\hat{H}_0 = \int dx \sum_{\alpha\sigma} \hat{\psi}_{\alpha\sigma}^\dagger \left[-\frac{\hbar^2}{2m} \nabla^2 + V(x) + \delta_{\alpha\sigma} \right] \hat{\psi}_{\alpha\sigma} + \int dx \sum_{\alpha} [M(x) \hat{\psi}_{\alpha\uparrow}^\dagger \hat{\psi}_{\alpha\downarrow} + \text{H.c.}], \quad (1)$$

where $\sigma = (\uparrow, \downarrow)$, $\psi_{\alpha\sigma}$ is the annihilation operator for atoms with spin σ in the α orbital, and $\delta_{\alpha\sigma}$ denotes the differential Zeeman shifts under an external magnetic field [32, 33]. The lattice potential $V(x) = V_0 \cos^2(k_0 x)$, and the Raman potential $M(x) = M_0 \cos(k_0 x)$, where both V_0 and M_0 are proportional to the AC polarizability of the clock states at the magic wavelength.

While high-band effects are generally important for Raman-assisted lattice SOC, a single-band tight-binding model is applicable when M_0 is not too large [34–37]. This can be satisfied by requiring $\Omega_1 \gg \Omega_2$, which allows us to write down the single-particle tight-binding model

$$\hat{H}_0 = -t_s \sum_{\langle i,j \rangle} (\hat{c}_{i\alpha\uparrow}^\dagger \hat{c}_{j\alpha\uparrow} - \hat{c}_{i\alpha\downarrow}^\dagger \hat{c}_{j\alpha\downarrow}) + \Gamma_z^\alpha \sum_i (\hat{n}_{i\alpha\uparrow} - \hat{n}_{i\alpha\downarrow}) + t_{so} \sum_i (\hat{c}_{i\alpha\uparrow}^\dagger \hat{c}_{i+1\alpha\downarrow} - \hat{c}_{i\alpha\uparrow}^\dagger \hat{c}_{i-1\alpha\downarrow} + \text{H.c.}), \quad (2)$$

where $\hat{c}_{i\alpha\sigma}$ is the annihilation operator for atoms on site- i with spin σ in the α orbital, t_s and t_{so} are respectively the spin-conserving and the spin-flipping hopping rates. Γ_z^α is the effective Zeeman field for the α orbital, which gives the energy shift resulting from the two-photon detuning of the corresponding Raman process. Note that Γ_z^α originates from the energy offset $\delta_{\alpha\sigma}$, and is different for the two orbitals at finite external magnetic fields. In the absence of interactions, the two orbitals are decoupled, and the ground state of the system, given $\Gamma_z^\alpha < 2t_s$, can be described by a pair of independent chiral topological insulators [28]. Such a chiral topological insulating state is an SPT state for free fermions of the AIII class, which is protected by $U(1)$ and chiral symmetries [38]. Under an open boundary condition, edge modes that are spin polarized along the $\pm x$ directions should emerge, which are robust against symmetry-preserving local perturbations.

A key ingredient in the system is the inter-orbital spin-exchange interactions in the clock-states manifolds [18–20]. In three dimensions, the interaction depends on whether the orbital degrees of freedom is singlet or triplet, with the scattering lengths of the two scattering channels given by a_{s-} and a_{s+} , respectively [25]. In a quasi-1D trapping potential and under a finite external magnetic field, the different scattering channels are

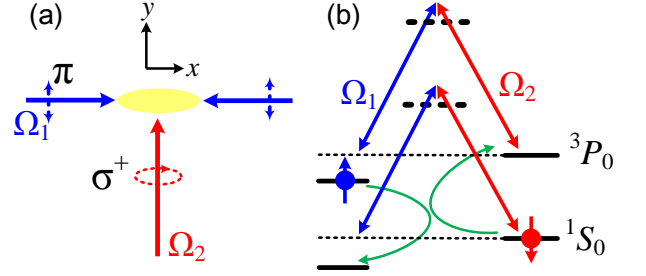


FIG. 1: Schematics of the system setup. (a) A quasi-1D atomic gas is subject to Raman lasers. (b) Raman level schemes in the clock-states manifold, with the blue-detuned Raman lasers at a magic wavelength. The green curve indicates the inter-orbital spin-exchange interaction. Note that the four nuclear spin states from 1S_0 and 3P_0 manifolds are isolated from the other nuclear spins, which can be achieved by imposing spin-dependent laser shifts [30].

coupled, and the interaction under the tight-binding approximation can be written as [29]

$$\hat{H}_{\text{int}} = V_{\text{ex}} \sum_i (\hat{c}_{ig\uparrow}^\dagger \hat{c}_{ie\downarrow}^\dagger \hat{c}_{ie\uparrow} \hat{c}_{ig\downarrow} + \text{H.c.}) + U \sum_i (\hat{n}_{ig\uparrow} \hat{n}_{ie\downarrow} + \hat{n}_{ig\downarrow} \hat{n}_{ie\uparrow}) + U_0 \sum_{i\sigma} \hat{n}_{ig\sigma} \hat{n}_{ie\sigma}, \quad (3)$$

where $\hat{n}_{i\alpha\sigma} = \hat{c}_{i\alpha\sigma}^\dagger \hat{c}_{i\alpha\sigma}$, U and U_0 are the Hartree-type on-site interactions, and V_{ex} is the on-site inter-orbital spin-exchange interaction. All the on-site interaction parameters $\{V_{\text{ex}}, U, U_0\}$ can be tuned via the external magnetic field through the orbital Feshbach resonance, or via the transverse trapping frequencies through the confinement induced resonance. Note that $U_0 = V_{\text{ex}} + U$ at zero external magnetic field [29].

As the interactions in Eq. (3) do not break the $U(1)$ or the chiral symmetries, the edge modes would not be gapped out in the presence of weak interactions, although the Z classification in the non-interacting case would be reduced to Z_4 [28, 39]. When the interaction strength, V_{ex} and U in particular, increases, the system may undergo an interaction-induced topological phase transition. To understand the effects of interaction on the topological properties of the system, in the following, we perform numerical simulations using density matrix renormalization group (DMRG) [40, 41] calculations, for which we retain 300 truncated states per DMRG block and perform 20 sweeps with a maximum truncation error $\sim 10^{-7}$.

Interaction-induced topological phase transition.— The topology of the system is reflected in the ground-state degeneracy of the entanglement spectrum, which is defined as $\xi_i = -\ln(\rho_i)$ [42–48]. Here, ρ_i is the eigenvalue of the reduced density matrix $\hat{\rho}_L = \text{Tr}_R |\psi\rangle\langle\psi|$, where $|\psi\rangle$ is the many-body ground-state wave function, and L, R correspond to the left or the right half of the 1D chain. We first study the topology of the system with increas-

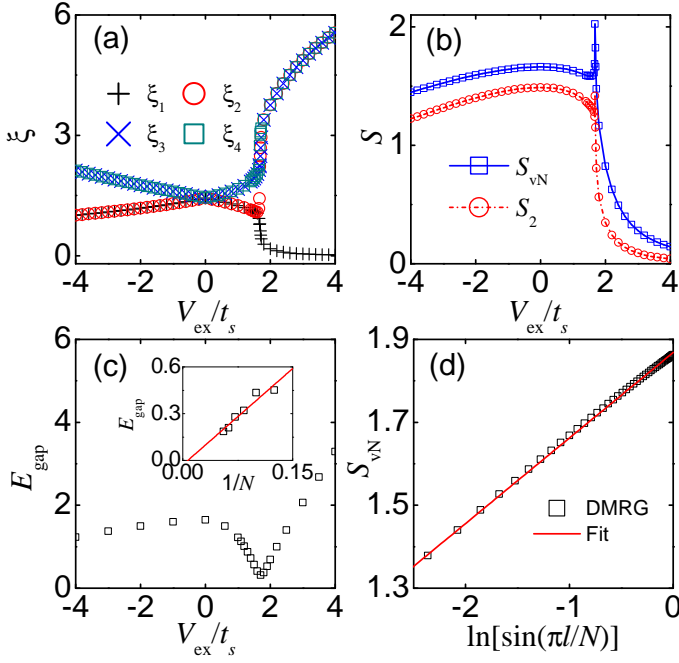


FIG. 2: (a) The lowest four levels in the entanglement spectrum ξ_i ($i = 1, 2, 3, 4$), and (b) the second-order Rényi entropy S_2 and the von Neumann entropy S_{vN} as functions of V_{ex}/t_s for a chain with $N = 60$ lattice sites at half filling with the atom number $M = 120$, and under open boundary conditions. (c) The bulk energy gap E_{gap} (the energy difference between the ground-state and the first excited state) for a chain with $N = 12$ lattice sites at half filling under the periodic boundary condition. (Inset) The bulk gap at the critical point as a function of $1/N$. The red solid line is a linear fit, with $E_{\text{gap}}/t_s \sim -0.02 \pm 0.05$ in the large- N limit. (d) The von Neumann entropy of a subchain of length l as a function of $\ln[\sin(\pi l/N)]$ for a chain with $N = 100$ sites at the critical point $V_{\text{ex}}/t_s = 1.693$ at half filling. The solid line is the linear fit with: $S_{\text{vN}} = 0.2 \ln[\sin(\pi l/N)] + 1.87$. The central charge is six times the slope of the linear fit. For all subplots, we fix $\Gamma_z^{g/e} = 0$, $U = 0$.

ing spin-exchange interaction V_{ex} while fixing $U = 0$ and $\Gamma_z^\alpha = 0$. In Fig. 2(a), we show the four lowest levels in the entanglement spectrum as functions of V_{ex}/t_s . While there is a four-fold degeneracy for the ground states in the entanglement spectrum with $V_{\text{ex}} = 0$, the degeneracy is partially lifted in the presence of weak V_{ex} . For repulsive bulk interactions ($V_{\text{ex}} > 0$), the ground state would no longer be degenerate beyond a critical interaction strength $V_{\text{ex}}^c/t_s \sim 1.69$, suggesting the existence of an interaction-induced topological phase transition. For attractive bulk interactions ($V_{\text{ex}} < 0$), the non-trivial SPT state persists even at large $|V_{\text{ex}}|$.

The existence and the location of the interaction-driven topological phase transition can be further confirmed by entropy and bulk-gap calculations. As demonstrated in Fig. 2(b), sharp features emerge at the critical point in both the second-order Rényi entropy $S_2 =$

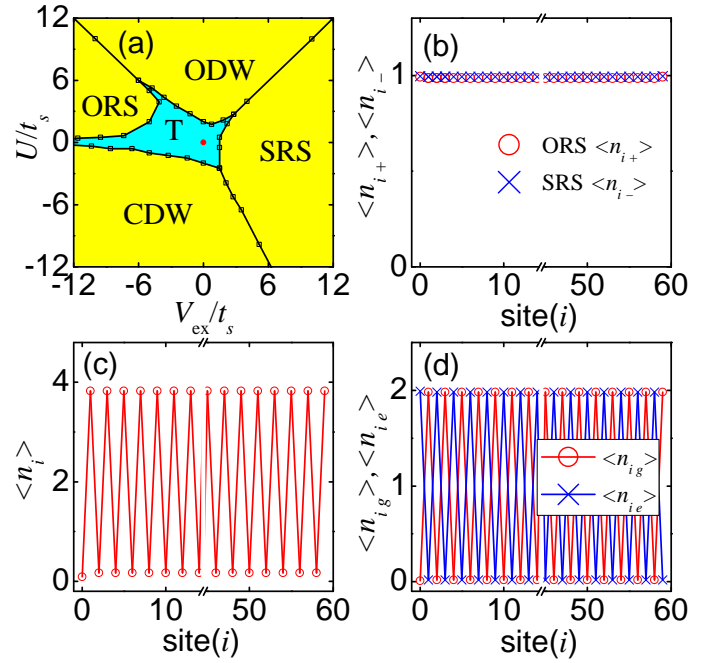


FIG. 3: (a) Phase diagram for a lattice with $N = 60$ sites at half filling, with $\Gamma_z^\alpha = 0$. (b) On-site densities of the states $|\pm\rangle$ in the ORS and SRS states, respectively, with $V_{\text{ex}}/t_s = -11$, $U/t_s = 5$ for ORS, and $V_{\text{ex}}/t_s = 8$, $U = 0$ for SRS. (c) Local atomic densities in the CDW state, with $\hat{n}_i = \sum_{\alpha\sigma} \hat{n}_{i\alpha\sigma}$, $V_{\text{ex}} = 0$, $U/t_s = -4$. (d) Local densities for different orbitals in the ODW state, with $\hat{n}_{i\alpha} = \sum_{\sigma} \hat{n}_{i\alpha\sigma}$, $V_{\text{ex}} = 0$, $U/t_s = 8$.

$-\log \text{Tr}(\hat{\rho}_L^2)$ [47–53], and the von Neumann entropy $S_{\text{vN}} = -\text{Tr}_L[\hat{\rho}_L \log \hat{\rho}_L]$. Whereas in Fig. 2(c), we show the bulk gap of a finite lattice with $N = 12$ and periodic boundary conditions at half filling. As the system goes across the critical point, the bulk gap closes in the thermodynamic limit (inset) and opens up again, which is typical of a continuous topological phase transition.

To characterize the topological phase transition, we further analyze the divergence of the von Neumann entropy at the critical point. In Fig. 2(d), we plot the von Neumann entropy of a subchain of length l as a function of $\ln[\sin(\pi l/N)]$. The linear behavior near $l = N/2$ suggests a logarithmic divergence of the entropy at the critical point, indicating a continuous topological phase transition. The central charge C of the phase transition can be extracted from the slope near $l = N/2$ [54, 55]. From Fig. 2(d), we estimate $C \sim 1.2$, which is close to that of a Luttinger liquid $C = 1$. Furthermore, we find that the spin-spin correlation $\langle \hat{S}_{i\alpha x} \hat{S}_{j\alpha x} \rangle$ ($\hat{S}_{i\alpha x}$ is the α -orbital spin operator along x on site i) exhibits a power-law decay at the critical point, with the coefficient ~ 1.38 [39]. A similar power-law decay, with a coefficient of ~ 2.1 , exists for correlations of the on-site density difference between the two orbitals, which can be regarded as the spin-spin correlation in the orbital degrees of freedom [39]. These results suggest that the system is a

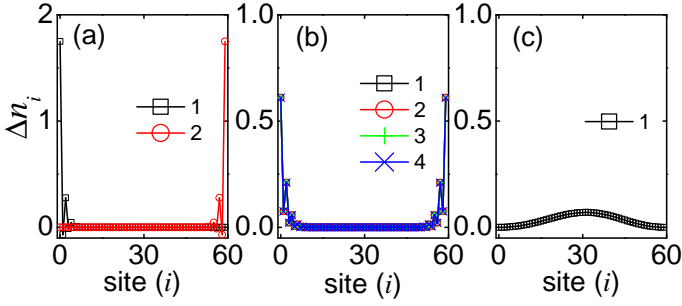


FIG. 4: The edge-mode density distributions Δn_i for (a) the T state with $V_{\text{ex}}/t_s = -1$, (b) the T state with $V_{\text{ex}}/t_s = 1$, and (c) the SRS state with $V_{\text{ex}}/t_s = 2$. Other parameters are the same as those in Fig. 2. The numbers in the figure legends label different edge modes in the degenerate subspace.

Luttinger liquid at the critical point.

Phase diagram and the trivial states.— Based on our understanding of the interaction-induced topological phase transition, we map out the phase diagram in Fig. 3. While the phase boundaries are determined from entanglement-spectrum and entropy calculations, we further identify different trivial states such as the rung-singlet states, the charge-density wave (CDW) state, and the orbital-density wave (ODW) state by calculating their corresponding local quantities [56–58]. As we have discussed previously, when $U = 0$, the ground state of the system can undergo a topological phase transition from a topological (T) phase to a trivial symmetric state. We define the singlet states in the orbital- (spin-) degrees of freedom as $|\pm\rangle = (|g \uparrow; e \downarrow\rangle \pm |g \downarrow; e \uparrow\rangle)/\sqrt{2}$, and analyze the local quantity $\langle \hat{n}_{i\pm} \rangle$, where $\hat{n}_{i\pm}$ is the local density operator for the corresponding singlet states. As indicated in Fig. 3(b), the trivial symmetric state for the repulsive V_{ex} case (with $U = 0$) is essentially a spin rung-singlet (SRS) state in a ladder system [58], which can be described by the direct-product state $\prod_i |-\rangle_i$. As U becomes finite, the system can become the orbital rung-singlet (ORS) state ($\prod_i |+\rangle_i$), the CDW, or an ODW state beyond the topological phase transition. Both the CDW and ODW are ordered trivial states with spontaneously broken chiral symmetry, which can be confirmed by calculating the corresponding local quantities as shown in Fig. 3(c)(d). In general, the phase diagrams are consistent with the understanding that the topology should be robust against weak symmetry-preserving interactions, while larger interactions would induce a topological phase transition, beyond which the system becomes trivial. Interestingly, the T state seems to persist in the large attractive V_{ex} limit, as long as $U = 0$. We also note that the overall topologies of the phase diagram are similar at finite Zeeman fields Γ_z^α .

Topological edge modes.— When the system is in the T state, topological edge modes should emerge at the boundaries, which significantly affect the ground-state

degeneracy at half filling. From numerical studies, we find that the ground-state degeneracy is dependent on the bulk interactions. At half filling, half of the four spin-polarized fermionic edge modes (two for each edge) should be occupied. The ground state in the absence of interactions should then be six-fold. However, the degeneracy of the ground state would change under finite interactions, leading to the splitting of the edge modes as well as the shifting of their energies. The ground-state degeneracy as well as the SPT classification can be clarified by invoking the projective representation of the relevant symmetry group [39]. We find that for repulsive bulk interactions $V_{\text{ex}} > 0$, the ground state at half filling are four-fold degenerate, with only one edge mode occupied on each edge. For attractive bulk interactions $V_{\text{ex}} < 0$, the ground state at half filling are two-fold degenerate, with the two edge modes at each edge either both empty or both occupied. This understanding of the topological edge modes not only provides a way to manipulate the edge modes by tuning the bulk interactions, but also offers a detection scheme of the SPT state based on the topological edge modes [59].

Detection.— The interaction-induced topological phase transition can be probed by measuring the local density distributions of the topological edge modes. The density distribution of the edge modes can be calculated as $\Delta n_i = \sum_{\alpha\sigma} \langle \hat{n}_{i\alpha\sigma}(2N) - \hat{n}_{i\alpha\sigma}(2N-2) \rangle$, where $\langle \hat{n}_{i\alpha\sigma}(M) \rangle$ is the expectation value of the density operator $\hat{n}_{i\alpha\sigma}$ under the bulk ground-state wave function for M atoms. As shown in Fig. 4, while the trivial SRS state features a non-local density distribution with negligible population at the edges, T states with two- and four-fold ground-state degeneracies feature localized density distributions at the edges. In particular, for T states with two-fold ground-state degeneracy, the localized edge-mode density distribution is twice as much as the state with four-fold degeneracy. We have checked that other trivial states have similarly negligible population at the edges as the SRS. Thus, the local density distribution of the edge modes not only allows for the detection of the interaction-induced topological phase transition, but also enables the determination of the edge-mode degeneracy in the T state. To measure the local atomic density distribution at the edges, one needs to measure the overall occupation of the $|g\rangle$ and the $|e\rangle$ orbitals at the boundaries. Measurement of populations of the $|g\rangle$ and $|e\rangle$ orbitals can be achieved, respectively, by coupling the 1S_0 - 1P_1 and the 3P_0 - 3P_1 (or the 3P_0 - 3S_1 - 1P_1 two-photon) transitions, and recording the resulting fluorescence. To selectively apply local operations at the edges, a localized laser field can be applied at the edges to provide the necessary energy shifts. Finally, we note that the topological phase transition may also be detected by probing the non-local string-order parameters [60], which can be achieved by measuring single-site-resolved on-site parity of the atom number [61].

Final remarks.— We have shown that SPT for interacting fermions can be realized and probed in alkaline-earth-like atomic gases. The scheme is facilitated by the separation of orbital and nuclear-spin degrees of freedom in the clock-state manifolds, and by the inter-orbital nuclear-spin-exchange interactions inherent in the system. An alternative scheme with separate Raman lasers for different orbitals can also be considered, in which case the reflection symmetry between the two orbitals would be broken even at a zero external magnetic field. However, the non-trivial SPT should survive, as it is not protected by the inter-orbital reflection symmetry. Our results open up the avenue for simulating SPT states for interacting fermions, and for studying SPT classifications using cold atoms.

Acknowledgments.— We thank Gyu-Boong Jo and Thomas Quella for helpful comments. This work is supported by the National Key R&D Program (Grant No. 2016YFA0301700), NKBEP (2013CB922000), the National Natural Science Foundation of China (Grant Nos. 60921091, 11274009, 11374283, 11422433, 11434007, 11434011, 11522436, 11522545, 11574392, 11674200), and the Research Funds of Renmin University of China (10XNL016, 16XNLQ03). X. Z. and G. C. are supported by the FANEDD under Grant No. 201316, SFSSSP; OYTPSP, and SSCC. W. Y. acknowledges support from the “Strategic Priority Research Program(B)” of the Chinese Academy of Sciences, Grant No. XDB01030200.

* Electronic address: liuzxphys@ruc.edu.cn

† Electronic address: wzhangl@ruc.edu.cn

‡ Electronic address: wyiz@ustc.edu.cn

§ Electronic address: chengang971@163.com

- [1] Z.-G. Gu and X.-G. Wen, Phys. Rev. B **80**, 155131 (2009).
- [2] F. Pollmann, E. Berg, A. M. Turner, and M. Oshikawa, Phys. Rev. B **85**, 075125 (2012).
- [3] X. G. Wen, Phys. Rev. B **40**, 7387 (1989).
- [4] X. G. Wen and Q. Niu, Phys. Rev. B **41**, 9377 (1990).
- [5] X. G. Wen, Int. J. Mod. Phys. B **B4**, 239 (1990).
- [6] F. D. M. Haldane, Phys. Rev. Lett. **50**, 1153 (1983); Phys. Lett. A **93**, 464 (1983).
- [7] C. L. Kane and E. J. Mele, Phys. Rev. Lett. **95**, 146802 (2005).
- [8] B. A. Bernevig and S.-C. Zhang, Phys. Rev. Lett. **96**, 106802 (2006).
- [9] J. E. Moore and L. Balents, Phys. Rev. B **75**, 121306(R) (2007).
- [10] L. Fu, C. L. Kane, and E. J. Mele, Phys. Rev. Lett. **98**, 106803 (2007).
- [11] X.-L. Qi, T. Hughes, and S.-C. Zhang, Phys. Rev. B **78**, 195424 (2008).
- [12] M. Takamoto, F. L. Hong, R. Higashi, and H. Katori, Nature (London) **435**, 321 (2005).
- [13] A. D. Ludlow, M. M. Boyd, T. Zelevinsky, S. M. Foreman, S. Blatt, M. Notcutt, T. Ido, and J. Ye, Phys. Rev. Lett. **96**, 033003 (2006).
- [14] B. J. Bloom, T. L. Nicholson, J. R. Williams, S. L. Campbell, M. Bishof, X. Zhang, W. Zhang, S. L. Bromley, and J. Ye, Nature (London) **506**, 71 (2014).
- [15] C. Wu, J. Hu, and S.-C. Zhang, Phys. Rev. Lett. **91**, 186402 (2003).
- [16] T. Fukuhara, Y. Takasu, M. Kumakura, and Y. Takahashi, Phys. Rev. Lett. **98**, 030401 (2007).
- [17] A. V. Gorshkov, A. M. Rey, A. J. Daley, M. M. Boyd, J. Ye, P. Zoller, and M. D. Lukin, Phys. Rev. Lett. **102**, 110503 (2009).
- [18] X. Zhang, M. Bishof, S. L. Bromley, C. V. Kraus, M. S. Safronova, P. Zoller, A. M. Rey, and J. Ye, Science **345**, 1467 (2014).
- [19] G. Cappellini *et al.*, Phys. Rev. Lett. **113**, 120402 (2014); *ibid* **114**, 239903 (2015).
- [20] F. Scazza, C. Hofrichter, M. Höfer, P. C. De Groot, I. Bloch, and S. Fölling, Nat. Phys. **10**, 779 (2014); *ibid* **11**, 514 (2015).
- [21] K. Duivenvoorden and T. Quella, Phys. Rev. B **87**, 125145 (2013).
- [22] A. Roy and T. Quella, arXiv:1512.05229.
- [23] S. Kolkowitz, S. L. Bromley, T. Bothwell, M. L. Wall, G. E. Marti, A. P. Koller, X. Zhang, A. M. Rey, and J. Ye, arXiv:1608.03854.
- [24] L. F. Livi, G. Cappellini, M. Diem, L. Franchi, C. Clivati, M. Frittelli, F. Levi, D. Calonico, J. Catani, M. Inguscio, and L. Fallani, Phys. Rev. Lett. **117**, 220401 (2016).
- [25] R. Zhang, Y. Cheng, H. Zhai, and P. Zhang, Phys. Rev. Lett. **115**, 135301 (2015).
- [26] G. Pagano, M. Mancini, G. Cappellini, L. Livi, C. Sias, J. Catani, M. Inguscio, and L. Fallani, Phys. Rev. Lett. **115**, 265301 (2015).
- [27] M. Höfer *et al.*, Phys. Rev. Lett. **115**, 265302 (2015).
- [28] X.-J. Liu, Z.-X. Liu, and M. Cheng, Phys. Rev. Lett. **110**, 076401 (2013).
- [29] J. Xu, R. Zhang, Y. Cheng, P. Zhang, R. Qi, and H. Zhai, Phys. Rev. A **94**, 033609 (2016).
- [30] B. Song, C. He, S. Zhang, E. Hagiyeve, W. Huang, X.-J. Liu, and G.-B. Jo, arXiv:1608.00478.
- [31] V. A. Dzuba and A. Derevianko, J. Phys. B **43**, 074011 (2010).
- [32] S. G. Porsev, A. Derevianko, and E. N. Fortson, Phys. Rev. A **69**, 021403 (2004).
- [33] S. G. Porsev and A. Derevianko, Phys. Rev. A **69**, 042510 (2004).
- [34] J.-S. Pan, X.-J. Liu, W. Zhang, W. Yi, and G.-C. Guo, Phys. Rev. Lett. **115**, 045303 (2015).
- [35] L. Zhou and X. Cui, Phys. Rev. B **92**, 140502(R) (2015).
- [36] J.-S. Pan, X.-J. Liu, W. Zhang, W. Yi, and G.-C. Guo, arXiv:1509.02993.
- [37] J.-S. Pan, W. Zhang, W. Yi, and G.-C. Guo, Phys. Rev. A **94**, 043619 (2016).
- [38] As the particle numbers are conserved for both orbitals, the system actually features an additional U(1) symmetry, which is redundant and does not alter the properties of the SPT.
- [39] See Supplemental Materials for details.
- [40] S. R. White, Phys. Rev. Lett. **69**, 2863 (1992).
- [41] U. Schollwöck, Rev. Mod. Phys. **77**, 259 (2005).
- [42] J.-Z. Zhao, S.-J. Hu, and P. Zhang, Phys. Rev. Lett. **115**, 195302 (2015).
- [43] T. Yoshida, R. Peters, S. Fujimoto, and N. Kawakami, Phys. Rev. Lett. **112**, 196404 (2014).

- [44] A. M. Turner, F. Pollmann, and E. Berg, Phys. Rev. B **83**, 075102 (2011).
- [45] F. Pollmann, A. M. Turner, E. Berg, and M. Oshikawa, Phys. Rev. B **81**, 064439 (2010).
- [46] L. Fidkowski, Phys. Rev. Lett. **104**, 130502 (2010).
- [47] S. T. Flammia, A. Hamma, T. L. Hughes, and X.-G. Wen, Phys. Rev. Lett. **103**, 261601 (2009).
- [48] H. Li and F. D. M. Haldane, Phys. Rev. Lett. **101**, 010504 (2008).
- [49] M. B. Hastings, I. González, A. B. Kallin, and R. G. Melko, Phys. Rev. Lett. **104**, 157201 (2010).
- [50] A. J. Daley, H. Pichler, J. Schachenmayer, and P. Zoller, Phys. Rev. Lett. **109**, 020505 (2012).
- [51] D. A. Abanin and E. Demler, Phys. Rev. Lett. **109**, 020504 (2012).
- [52] H.-C. Jiang, Z.-H. Wang, and L. Balents, Nat. Phys. **8**, 902 (2012).
- [53] R. Islam, R. Ma, P. M. Preiss, M. E. Tai, A. Lukin, M. Rispoli, and M. Greiner, Nature (London) **528**, 77 (2015).
- [54] P. Calabrese and J. Cardy, J. Stat. Mech. **0406** 06002 (2004).
- [55] A. E. B. Nielsen, G. Sierra, and J. I. Cirac, Phys. Rev. A **83**, 053807 (2011).
- [56] V. Bois, S. Capponi, P. Lecheminant, M. Moliner, and K. Totsuka, Phys. Rev. B **91**, 075121 (2015).
- [57] V. Bois, P. Fromholz, and P. Lecheminant, Phys. Rev. B **93**, 134415 (2016).
- [58] S. Capponi, P. Lecheminant, and K. Totsuka, Ann. Phys. **367**, 50 (2016).
- [59] Z.-X. Liu, Z.-B. Yang, Y.-J. Han, W. Yi, and X.-G. Wen, Phys. Rev. B **86**, 195122 (2012).
- [60] K. Duivenvoorden and T. Quella, Phys. Rev. B **86**, 235142 (2012).
- [61] M. Endres, M. Cheneau, T. Fukuhara, C. Weitenberg, P. Schauss, C. Gross, L. Mazza, M. C. Banuls, L. Pollet, I. Bloch, and S. Kuhr, Science **334**, 200 (2011).

Supplemental Materials

A. Topological edge modes and the band structure

We calculate the band structure $\mu(M) = E_0(M+1) - E_0(M)$, which is essentially the energy required to add an atom to a system of M atoms. Here, $E_0(M)$ is the ground-state energy of M atoms on N lattice sites with open boundary conditions. As illustrated in Fig. S1(a), when the system is in the SPT state, mid-gap modes associated with the topological edge modes emerge in the band structure. These mid-gap modes represent the excitation energies required as the occupation number of the four topological edge modes (two for each orbital) increases sequentially from zero to four. As V_{ex} increases, these mid-gap modes would shift toward the bulk and eventually merge into the bulk spectrum. Such a behavior can be characterized by calculating the excitation energy gap between the bulk spectrum and the nearest mid-gap state: $\Delta\mu = [E_0(2N+3) - E_0(2N+2)] - [E_0(2N+1) - E_0(2N)]$, where $2N$ corresponds to the half-filling condition for a lattice with N sites. As illustrated in Fig. S1(b), the excitation gap vanishes at the critical point, indicating the merging of the mid-gap modes into the bulk spectrum.

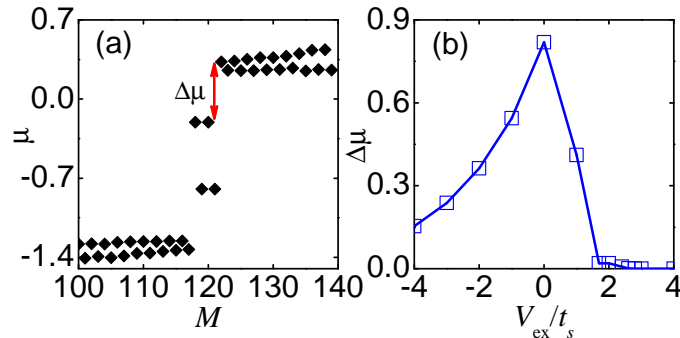


FIG. S1: (a) Band structure $\mu(M) = E_0(M+1) - E_0(M)$ as functions of V_{ex}/t_s for a chain with $N = 60$ lattice sites at half filling with the atom number $M = 120$, and under open boundary conditions. Here, $V_{\text{ex}}/t_s = -1$. (b) The excitation energy gap $\Delta\mu$ as a function of V_{ex}/t_s . For both plots, we have $\Gamma_z^{g/e} = 0$, $U = 0$, $U_0/t_s = -1$.

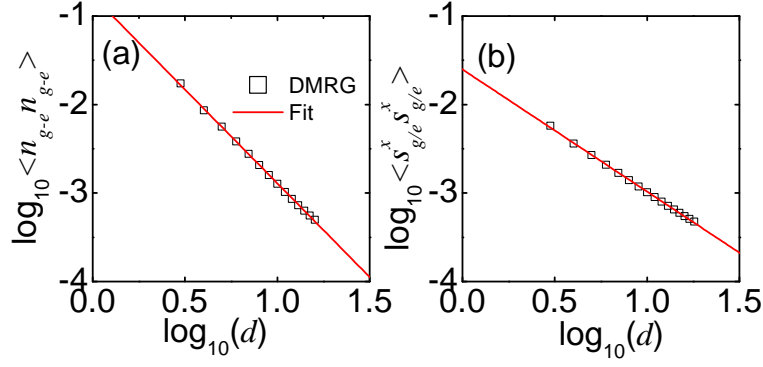


FIG. S2: (a) Power-law decay of the correlation of the density-difference at the critical point in Fig. 2(d) of the main text. The linear fit is given by $y = -2.1x - 0.77$. (b) Power-law decay of the spin-spin correlation at the same critical point. The linear fit is given by $y = -1.38x - 1.6$.

B. Characterizing the topological phase transitions

The continuous topological phase transition between the T state and the rung-singlet states can be characterized by the relevant correlation functions at the critical point. Taking the T-SRS boundary as an example, we find that the correlation of the on-site density difference between the two orbital, defined as $\langle \hat{n}_{g-e} \hat{n}_{g-e} \rangle = \langle (\hat{n}_{ig} - \hat{n}_{ie})(\hat{n}_{i+d,g} - \hat{n}_{i+d,e}) \rangle$, exhibits a power-law decay at the phase boundary. Similarly, the spin-spin correlation, $\langle \hat{S}_{g/e}^x \hat{S}_{g/e}^x \rangle = \langle \hat{S}_{i,\alpha x} \hat{S}_{i+d,\alpha x} \rangle$, also decays in a power-law fashion at the critical point. Here, $\hat{S}_{i,\alpha x} = \sqrt{2}/2(\hat{c}_{i\alpha\uparrow}^\dagger \hat{c}_{i\alpha\downarrow} + H.c.)$. In Fig. S2, we show the linear fit on a log-log plot of the correlations functions versus the distance between sites d . The power-law decay of the correlations functions, combined with the central charge calculation, suggest that the system is a Luttinger liquid at the critical point.

Similarly, we find that the topological phase transitions between the T state and the CDW, the ODW, and the ORS states are all continuous. As shown in Fig. S3, by characterizing the divergence of the von Neumann entropy at the corresponding phase boundaries, we find that the central charges for the T-ORS, the T-ODW, and the T-CDW phase transition are ~ 0.96 , ~ 0.86 , and ~ 0.90 , respectively.

C. Projective representation of the SPT state

In this section, we discuss the projective representation of the SPT state in the main text, which determines the classification of the SPT state, how the edge states vary under the symmetry operations, and sheds light on the edge-modes degeneracy. As discussed in the main text, for a single chain, i.e. with only one orbital degree of freedom, the left edge mode $|\psi_l\rangle$ is an eigenstate of the spin operator $\hat{S}_x = \hat{\sigma}_x/2$ with the eigenvalue $+1/2$ (we have taken \hbar to be one), and the right edge mode $|\psi_r\rangle$ is an eigenstate of \hat{S}_x with the eigenvalue $-1/2$,

$$\hat{S}_x |\psi_l\rangle = \frac{1}{2} |\psi_l\rangle, \quad \hat{S}_x |\psi_r\rangle = -\frac{1}{2} |\psi_r\rangle. \quad (S1)$$

So we can describe the edge modes by fermion operators \hat{c}_{1l} and \hat{c}_{1r} , $|\psi_l\rangle = \hat{c}_{1l}^\dagger |\text{vac}\rangle$, $|\psi_r\rangle = \hat{c}_{1r}^\dagger |\text{vac}\rangle$ respectively. Here the subscript 1 indicate the orbital degree of freedom.

Without loss of generality, we only consider the left boundary. The edge mode varies under symmetry action as the following:

$$\hat{U}(\theta) \hat{c}_{1l} \hat{U}(\theta)^{-1} = e^{i\theta} \hat{c}_{1l}, \quad (S2)$$

$$(\hat{\mathcal{C}}\mathcal{T}) \hat{c}_{1l} (\hat{\mathcal{C}}\mathcal{T})^{-1} = \hat{c}_{1l}^\dagger. \quad (S3)$$

The fermion mode \hat{c}_{1l} span a two-dimensional Hilbert space $|0\rangle$ and $|1\rangle = \hat{c}_{1l}^\dagger |0\rangle$. In this two-dimensional Hilbert space of the left edge states, we can replace \hat{c}_{1l} and \hat{c}_{1l}^\dagger as $\hat{\sigma}^- = (\hat{\sigma}_x - i\hat{\sigma}_y)/2$ and $\hat{\sigma}^+ = (\hat{\sigma}_x + i\hat{\sigma}_y)/2$, respectively.

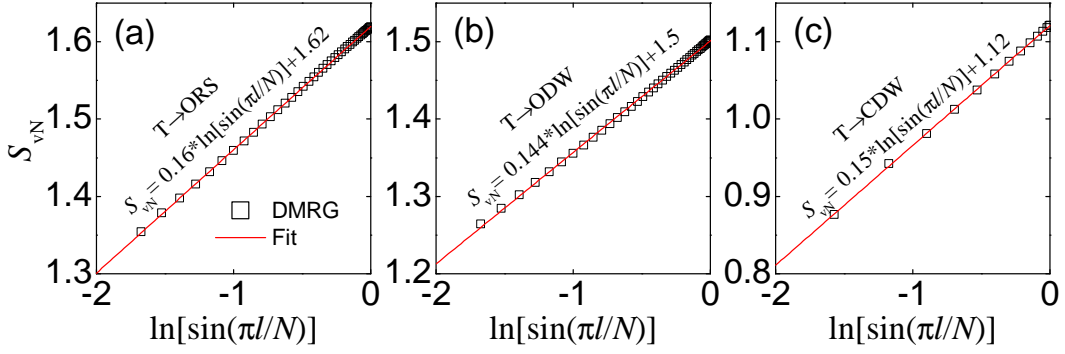


FIG. S3: The von Neumann entropy of a subchain of length l as a function of $\sin(\pi l/N)$ for a chain with $N = 100$ sites. (a) At the T-ORS phase boundary with $V_{\text{ex}}/t_s = -5$, $U/t_s = 2$; (b) at the T-ODW phase boundary with $V_{\text{ex}}/t_s = -1.19$, $U/t_s = 2.81$; (c) at the T-CDW boundary with $V_{\text{ex}}/t_s = -5$, $U/t_s = -1$.

From Eqs. (S2) and (S3), we can solve the matrix form of symmetry action as

$$\hat{U}(\theta) \rightarrow M_1(\theta) = \begin{pmatrix} 1 & 0 \\ 0 & e^{i\theta} \end{pmatrix}, \quad (\text{S4})$$

$$(\hat{\mathcal{C}}\mathcal{T}) \rightarrow M_1(\mathcal{C}\mathcal{T}) = \hat{\sigma}_x K. \quad (\text{S5})$$

Since $M_1(\mathcal{C}\mathcal{T})K M_1(\theta) = e^{-i\theta} M_1(\theta) M_1(\mathcal{C}\mathcal{T})K$, these matrices form a projective representation of the symmetry group $U(1) \times Z_2^T$, and they describe how the edge state vary under the action of the symmetry operations.

Now we consider a two-leg ladder, i.e. with both orbital degrees of freedom, as discussed in the main text. The edge modes of the second chain located at the left and the right edge can be described as \hat{c}_{2l} and \hat{c}_{2r} , respectively. Now at the left edge we have two fermionic zero modes \hat{c}_{1l} and \hat{c}_{2l} . The Hilbert space spanned by the left edge states is four-dimensional. Since $\{\hat{c}_{1l}, \hat{c}_{2l}\} = 0$, now the fermion operators should be replaced by

$$\hat{c}_{1l} = I \otimes \hat{\sigma}^-, \quad \hat{c}_{2l} = \hat{\sigma}^- \otimes \hat{\sigma}^z, \quad (\text{S6})$$

the last operator $\hat{\sigma}^z$ ensures that \hat{c}_{1l} and \hat{c}_{2l} are anti-commuting.

Since the symmetry acts on the fermion operators as follows,

$$U(\theta)\hat{c}_{\alpha l}U(\theta)^{-1} = e^{i\theta}\hat{c}_{\alpha l}, \quad (\text{S7})$$

$$(\mathcal{C}\mathcal{T})\hat{c}_{\alpha l}(\mathcal{C}\mathcal{T})^{-1} = \hat{c}_{\alpha l}^\dagger, \quad (\text{S8})$$

we can solve the representation matrix of the symmetry operations as

$$\hat{U}(\theta) \rightarrow M_2(\theta) = \begin{pmatrix} 1 & 0 \\ 0 & e^{i\theta} \end{pmatrix} \otimes \begin{pmatrix} 1 & 0 \\ 0 & e^{i\theta} \end{pmatrix}, \quad (\text{S9})$$

$$(\hat{\mathcal{C}}\mathcal{T}) \rightarrow M_2(\mathcal{C}\mathcal{T}) = \hat{\sigma}_y \otimes \hat{\sigma}_x K. \quad (\text{S10})$$

The above matrices can be simultaneously block-diagonalized as

$$M_2(\theta) = \begin{pmatrix} 1 & & \\ & e^{2i\theta} & \\ & & e^{i\theta} \\ & & & e^{i\theta} \end{pmatrix}, \quad (\text{S11})$$

$$M_2(\mathcal{C}\mathcal{T}) = \begin{pmatrix} \hat{\sigma}_y & \\ & -\hat{\sigma}_y \end{pmatrix} K, \quad (\text{S12})$$

which is a direct sum of two irreducible projective representations (of the same class).

At half filling, only two of the four edge modes are occupied. The ground states should then be six-fold degenerate in the absence of interactions. If the effective interaction between the two legs is repulsive, there is always one fermion

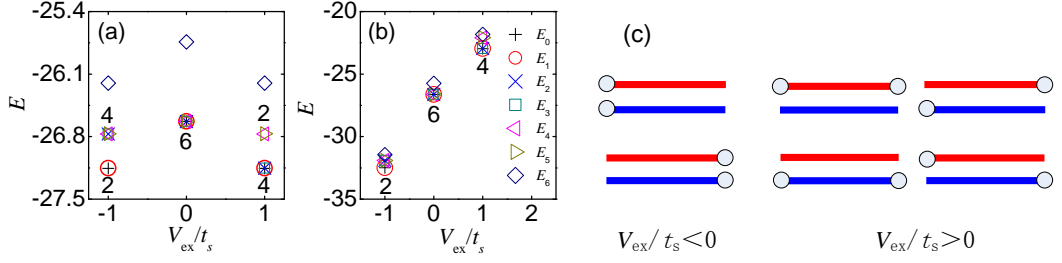


FIG. S4: Ground state degeneracy for a finite chain with $N = 10$ at half filling. (a) $U_0 = 0$ and (b) $U_0 = V_{\text{ex}} + U$. We fix $U = 0$ here. (c) A schematic illustration of the occupied edge fermion modes of the degenerate ground states for different bulk interactions.

zero mode occupied at one edge, which is described by the irreducible projective representation

$$M_2(\theta) = \begin{pmatrix} e^{i\theta} & \\ & e^{i\theta} \end{pmatrix}. \quad (\text{S13})$$

$$M_2(\mathcal{CT}) = -\hat{\sigma}_y K. \quad (\text{S14})$$

In this case, the ground states at half filling feature a four-fold degeneracy. On the other hand, if the interaction is attractive, the fermion zero modes are either not occupied or doubly occupied at each edge, they are described by the irreducible projective representation

$$M_2(\theta) = \begin{pmatrix} 1 & \\ & e^{2i\theta} \end{pmatrix}, \quad (\text{S15})$$

$$M_2(\mathcal{CT}) = \hat{\sigma}_y K. \quad (\text{S16})$$

The ground states are then two-fold degenerate at half filling. Note that while the projective representation above indicates four ground states, only two of them are at half filling. By comparing numerical results with the theory above, we find that the repulsive effective interaction corresponds to a repulsive bulk spin-exchange interaction $V_{\text{ex}} > 0$, and the attractive effective interaction corresponds to an attractive bulk interaction $V_{\text{ex}} < 0$. This implies that when the bulk spin-exchange interactions are tuned, the ground-state degeneracy at half filling can change from two (for $V_{\text{ex}} < 0$) to six (for $V_{\text{ex}} = 0$) and finally to four (for $V_{\text{ex}} > 0$). This is illustrated in Fig. S4 for a finite chain with $N = 10$ at half filling.

Similarly, if one more chain is stacked into the ladder, then the resultant edge states can be described by the following projective representation,

$$M_3(\theta) = \begin{pmatrix} e^{im\theta} & \\ & e^{in\theta} \end{pmatrix}, \quad (\text{S17})$$

$$M_3(\mathcal{CT}) = \hat{\sigma}_y K, \quad (\text{S18})$$

with $m + n = \text{odd}$. Finally, if four chains are stacked together, then the edge states can be fully gapped out and it is described by a trivial projective representation. Thus, the fermionic SPT phases have Z_4 classification and there is only one root phase.